

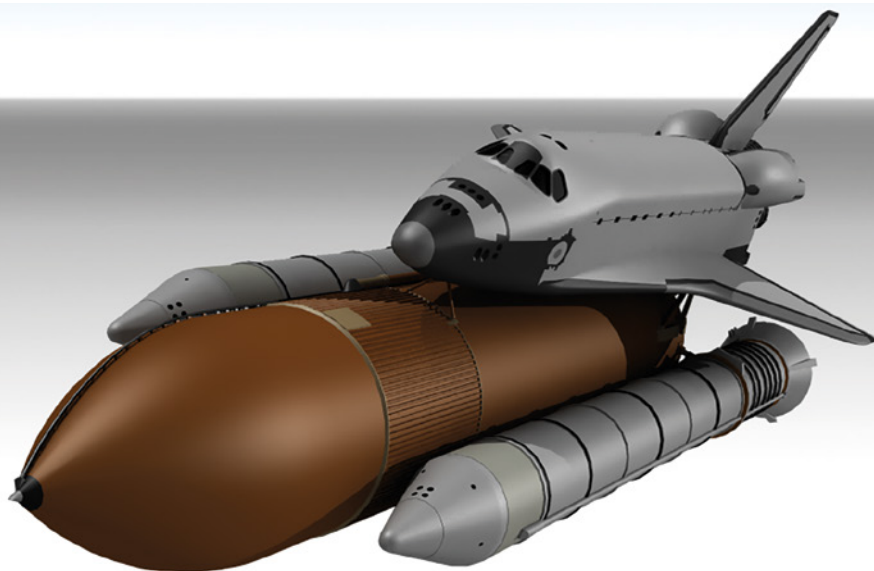
A Study of Aerothermal Loads

in the Presence of Edney Type IV Interaction

By Dr. Leonid Gurov, Dr. Andrey Ivanov, Mentor, a Siemens Business

The simulation of supersonic flow over aircraft is usually focused on shockwave drag and aerothermal loads estimation. For hypersonic vehicles, where aerodynamic heating becomes more prominent, the accurate prediction of the latter is essential in order to design an efficient Thermal Protection System (TPS). If the analyzed geometry represents real prototype of the vehicle (rather than some simplified model) one can expect a highly complex flow structure that includes multiple shockwaves, expansion fans and contact discontinuities. Under these conditions the interaction between the shocks and boundary layer flow may lead to localized heat fluxes that are several times higher than the ones at the stagnation point. This article gives an account of the FloEFD simulations, where such effects are known to occur.





The investigation of shock/shock interaction in a 2D supersonic flow around a cylinder with an impinging shock generated by a wedge gives a good understanding of the processes affecting the surface heat transfer. Depending on the relative coordinates of the point where the wedge shock crosses the cylinder bow shock, six types of interaction [1] are possible (Figure 1). Two cases that draw most attention are known as “Type III” and “Type IV” interactions, where the oblique shock crosses the normal shock. Such interactions should be avoided as they lead to the most significant increase of heat flux. A mixing layer impinges on the body surface in the first case, while the second case is notable for the formation of a small-scale supersonic jet that penetrates a region of low subsonic flow. The remaining four “types” have a minor effect.

To demonstrate how the peak values of pressure and heat flux vary with the change of shock interaction type and freestream conditions, a set of experimental measurements [2] were initiated after testing early layout of the Space Shuttle system (for its main elements, see Figure 2), where extremely high heat fluxes were detected on the Orbiter nose. Obviously, External Tank played the part of the wedge here and resulted in Type III/IV interaction near the nose. Ever since the 2D shock/shock interaction problem has become a well-known benchmark test case. Such a test is considered in the first part of this article.

The second part is focused on the study of Type IV interaction near the nose of the actual Space Shuttle Orbiter. It should be noted that the “Final” layout of this system minimizes the

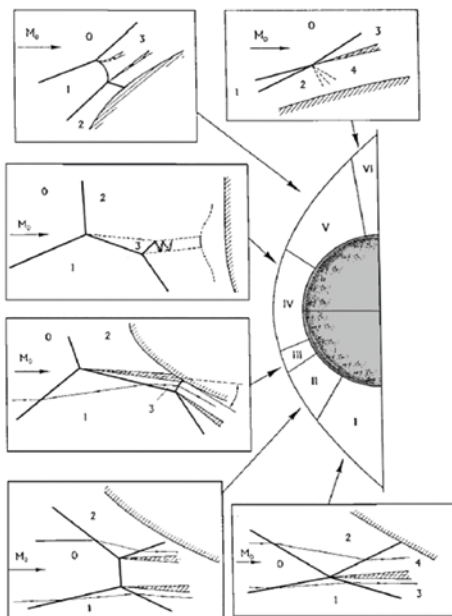


Figure 1. Six types of shock/shock interaction as classified by Edney [1]

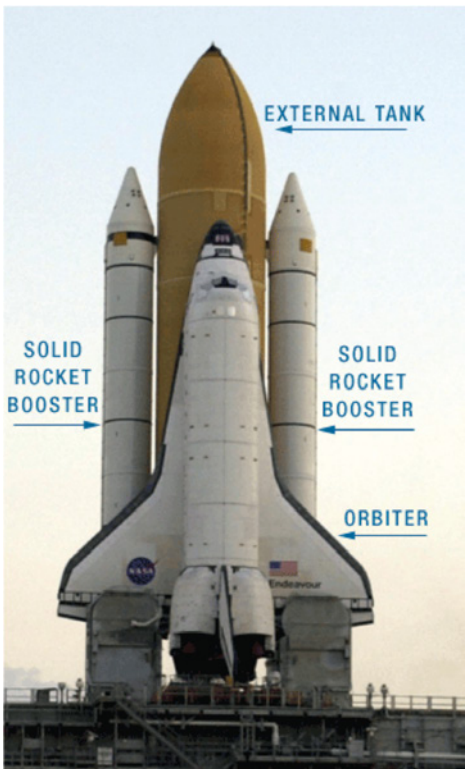


Figure 2. Space Shuttle system with its main elements

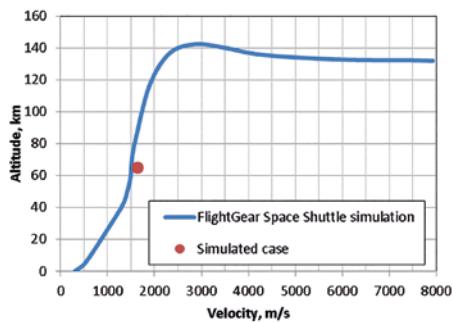


Figure 3. Dependencies of Space Shuttle flight altitude on velocity

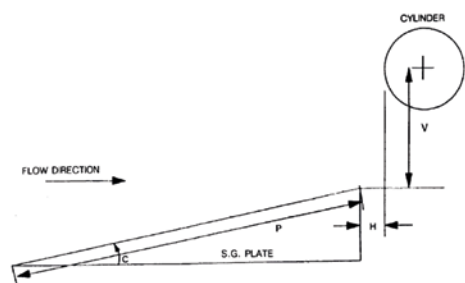


Figure 4. Schematic diagram of the shock/shock interaction model [2]



Figure 5. Mach number contours

probability of such an incident. To be more specific, when the velocity of vehicle is about Mach 5 to 10 and the pitch angle is close to zero, the oblique shock does not cross the normal shock near the Orbiter nose, so one can expect a Type V/VI interaction at most. Further acceleration (up to $M=25$) occurs at the altitude of approximately 100km (Figure 3), where the mean free path of a particle is of the same scale (≈ 1 m) as the actual vehicle size, obviously such cases cannot be handled by Navier-Stokes equations. Moreover, the External Tank is discarded at the altitude of 113 km. As a compromise a special case is considered, where the pitch angle is assumed to be well below zero and the flight conditions correspond to the altitude of 65km (solid boosters are discarded at the altitude of 45km).

Case 1 - Shock/shock interaction in a 2D flow around circular cylinder

This validation case demonstrates FloEFD capabilities to predict surface heat flux in the presence of shock/shock interaction. The input data for the calculation was taken from [2] and corresponded to the experimental run #20. Figure 4 shows the original experimental layout, where a 3-inch-diameter cylinder was used. In the considered case, $V=2.78$ in, $H=0.5$ in, $P=26.5$ in and $C=10^\circ$.

The freestream conditions were as follows: $p_\infty=0.06607$ psia, $T_\infty=126.8$ K; $M_\infty=7.944$. Wall temperature was fixed to 294.4K.

A uniform square mesh was used to discretize computational domain with the characteristic cell size being 1/150 of cylinder diameter. To attain stable shock structure, "time-dependent" option was enabled.

Figure 5 shows the Mach number contours over the whole computational domain. A Mach 2 jet near cylinder is prominent and indicates the Type IV interaction. The comparison with the available Schlieren

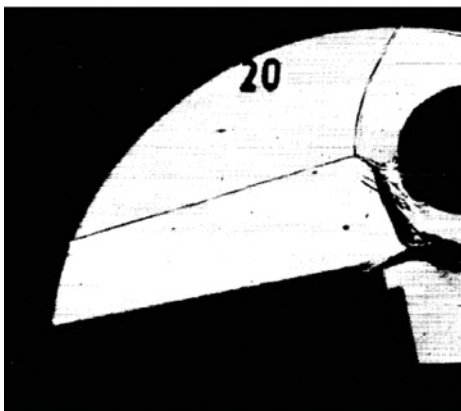


Figure 6a

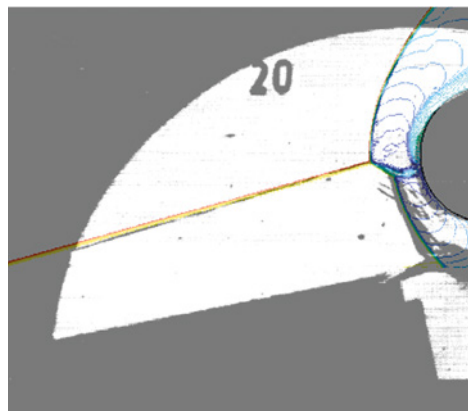


Figure 6b

Figure 6. Schlieren photography as taken from [2] (a) and merged with Mach number isolines (b)

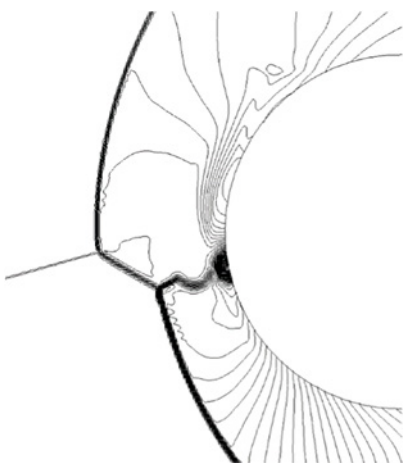


Figure 7a

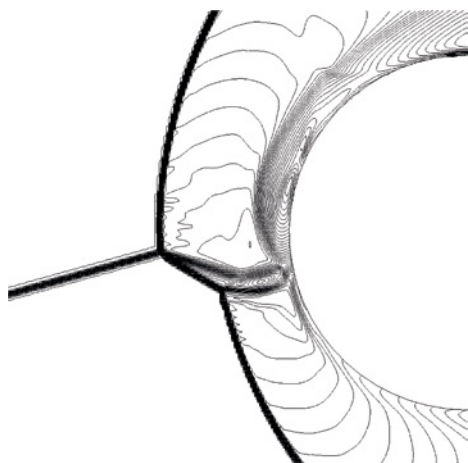


Figure 7b

Figure 7. Isolines of pressure (a) and Mach number (b) near cylinder

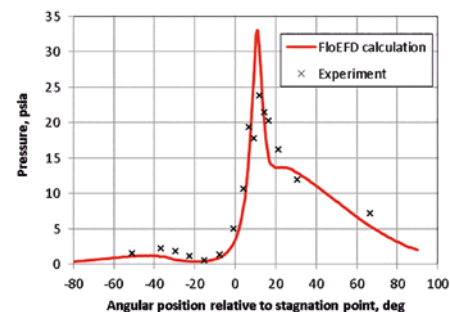


Figure 8. Pressure distribution over cylinder surface

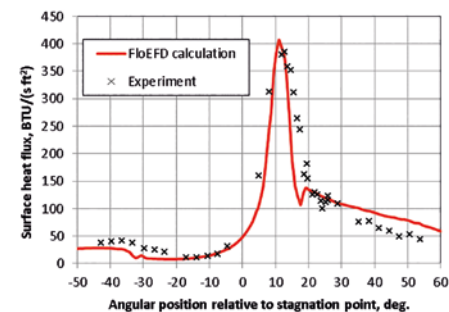


Figure 9. Heat flux distribution over cylinder surface

photography shows good agreement with the experiment in terms of flow structure (Figure 6).

Let us study the flow near the cylinder in more detail by plotting pressure and Mach number isolines (Figure 7). According to these plots, the size of the produced jet in a transverse direction is about 1/20 of cylinder diameter. From the top and bottom sides it is 'bounded' by a contact discontinuity. Before reaching the cylinder jet passes through a series of oblique shocks and a terminal normal shock. The resulting flow splits into two halves; the one in the upper direction accelerates and becomes supersonic, while the flow in the lower direction remains subsonic.

Figure 8 shows the comparison between the calculated and measured pressure distributions around the cylinder. One can see a good agreement with experiment in terms of peak pressure relative coordinate, although the actual value is a bit over-predicted.

The corresponding distribution of heat flux (Figure 9) shows good agreement with experiment in terms of both, peak value and its relative coordinate. As a matter of fact, the obtained peak value (400 BTU/ ft2·s) is almost 13 times larger comparing to the estimated value at the stagnation point (30 BTU/ft2·s) in case of the symmetry flow around cylinder (no shock interaction).

The increase of heat flux at the angular position of -30° is due to laminar-turbulent transition in the boundary layer. Although minor, this effect was captured in the calculation. Similar transition is observed at the angular position of 25°. One can notice that the predicted laminar-turbulent transition is shifted 5° towards the stagnation point. Such error can be considered insignificant.

Case 2 - Flow over space shuttle orbiter with external tank

While the preceding case was mainly focused on the quantitative flow analysis keeping the CAD model as simple as possible, this case is notable for the complex geometry analyzed. To perform the simulation it was convenient to use a CAD model of the Space Shuttle available online [3]. In order to attain the angle of the oblique shock generated by the External Tank so that it could cross the normal shock near the Orbiter nose and, thus, result in type IV interaction the external flow Mach number was set to 5.6, while the pitch angle was adjusted to -23°. The freestream conditions corresponded to the altitude of 65 km ($p_\infty=9.922\text{ Pa}$; $T_\infty=231.45\text{ K}$).

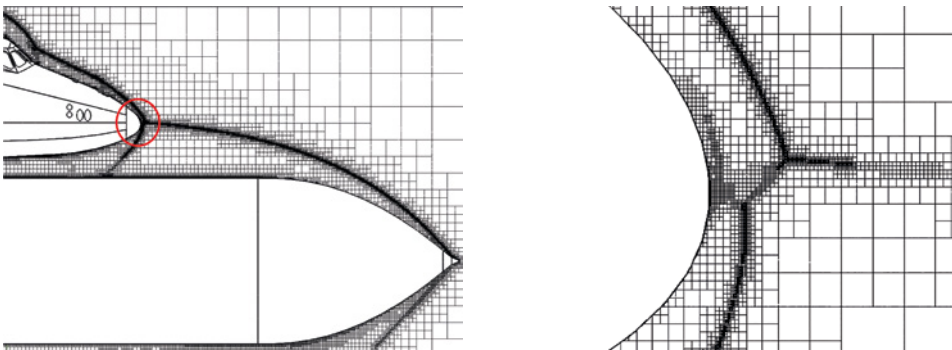


Figure 10. Computational mesh generated after Solution-Adaptive Refinement

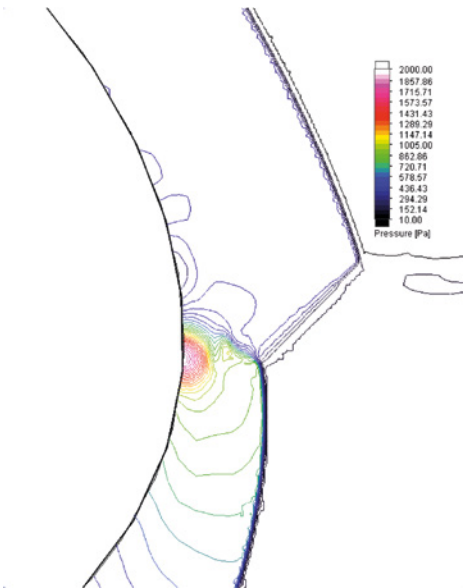


Figure 11a

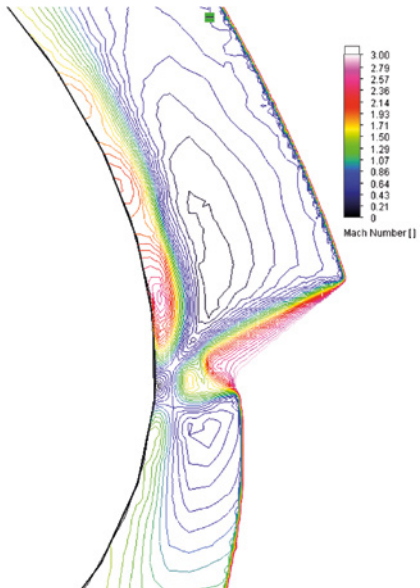


Figure 11b

Figure 11. Isolines of pressure (a) and Mach number (b) near the Orbiter nose

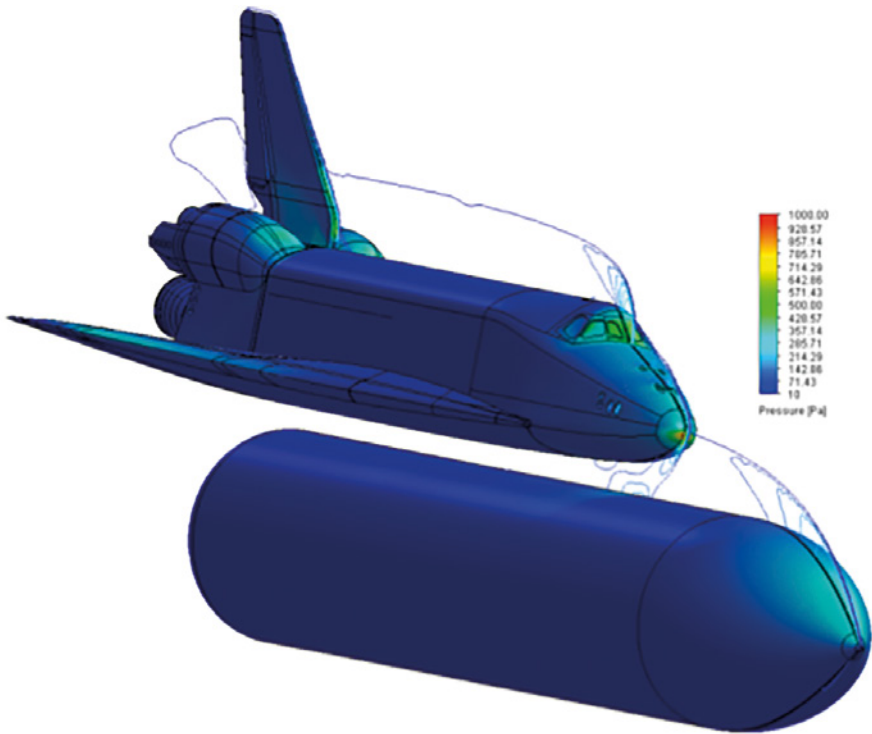


Figure 12. Surface pressure and pressure isolines in the symmetry plane

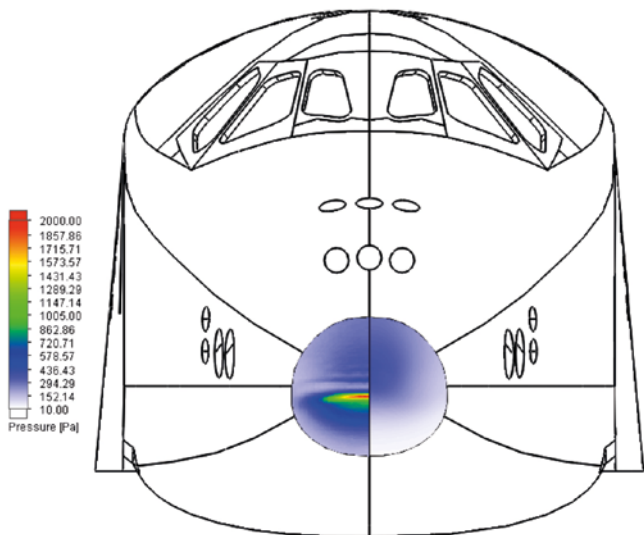


Figure 13. Pressure distribution along the Orbiter nose in the presence of Type IV shock/shock interaction (left) and in case of single Orbiter flow (right)

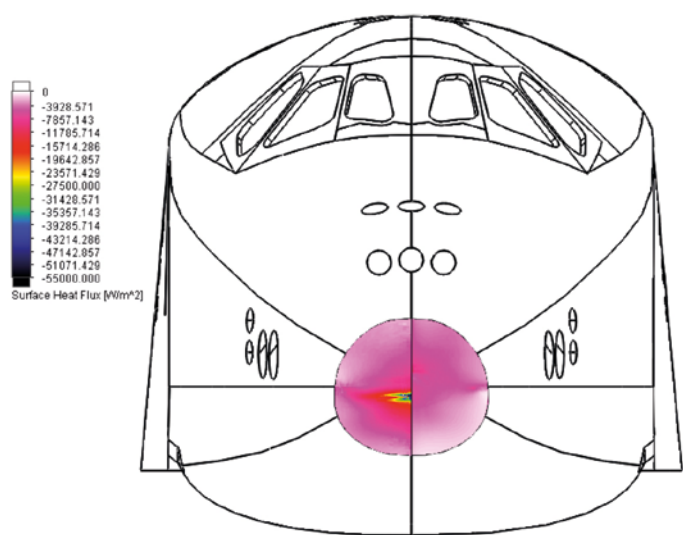


Figure 14. Heat flux distribution along the Orbiter nose in the presence of Type IV shock/shock interaction (left) and in case of single Orbiter flow (right)

While preparing the geometry, specifying mesh settings and boundary conditions several assumptions were made that helped to reduce the overall CPU time for analysis. These had only minor effect on the accuracy of the solution in the regions of interest.

A uniform half-symmetry mesh was used, where the characteristic cells size in the basic mesh was about 1/5 of the External Tank diameter. To refine mesh in the regions of interest (impinging shock, Orbiter bow shock, etc.), Solution-Adaptive Refinement (SAR) was used. The resulting mesh obtained after running SAR seven times comprised of about five million cells (Figure 10). The calculation was stopped after obtaining the converged values of the following surface goals specified on the Orbiter nose – min/max pressure, average surface heat flux.

Figure 11 shows the pressure and Mach number isolines near the Orbiter nose. Comparing to the preceding case, the supersonic jet turned out to be shorter in length; still, the ‘bounding’ contact discontinuities and a terminating normal shock can be easily distinguished.

The pressure contours plotted over the whole Orbiter surface (Figure 12) give a good idea of the size of the region, where pressure increase caused by Type IV shock/shock interaction is prominent. Comparing to the results obtained in the flow analysis around the single Orbiter (Figure 13-14), the presence of Type IV interaction leads to the increase of peak pressure and heat flux values by 5.5 times (Figure 15). A larger quantitative difference was observed in the preceding case. That was partly due to the larger Mach number of the external flow.

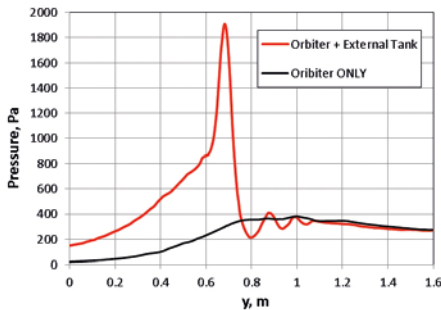


Figure 15a

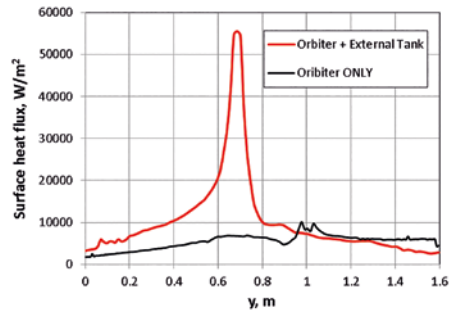


Figure 15b

Figure 15. Distributions of pressure (a) and heat flux (b) along the nose in the symmetry plane

Summary

The effect of heat transfer rate increase caused by Edney type IV shock/shock interaction has been investigated with FloEFD. A well-known benchmark case was used for the initial test that showed good agreement with experimental data in terms of flow structure, surface pressure and heat flux distributions. The results obtained in the FloEFD analysis of Space Shuttle revealed a small-scale region on the Orbiter nose with a moderate increase of surface heat transfer rate caused by type IV interaction.

References

[1] Edney, B., “Anomalous heat transfer and pressure distributions on blunt bodies at hypersonic speeds in the presence of an impinging shock”, FFA Report 115, Aero. Res. Institute of Sweden, 1986

[2] Holden, M. S. et. al., “Studies Of Aerothermal Loads Generated in Regions Of Shock/Shock Interaction In Hypersonic Flow”, AIAA paper 88-0477, Jan 1988.

[3] <http://www.grabcad.com>



Mentor
A Siemens Business

This article originally appeared in
Engineering Edge Vol. 7 Iss. 1

Download the latest issue:
www.mentor.com/products/mechanical/engineering-edge

©2018 Mentor Graphics Corporation, all rights reserved. This document contains information that is proprietary to Mentor Graphics Corporation and may be duplicated in whole or in part by the original recipient for internal business purposes only, provided that this entire notice appears in all copies. In accepting this document, the recipient agrees to make every reasonable effort to prevent unauthorized use of this information. All trademarks mentioned in this publication are the trademarks of their respective owners.

ENGINEERING EDGE

Accelerate Innovation
with CFD & Thermal
Characterization

You might also be interested in...

Thermal Simulation of a SYN TRAC Powerpack

Edge Devices are Hot for IoT

Distributed Chilled Water Pumping AC System

Reliability Evaluation of Sintered Copper Die Bonding Materials

Virtual Reality and Modeling Tools

Ask the GSS Expert

Simulation of Hydraulic Servo Gimbal Control of a Space Launch Vehicle

How to... Convert CAD Geometry into a FloMASTER Sub-System

Development of a Turbocharger with FloEFD

Risk Prevention & Energy Saving in Ships

Interview: Takuya Shinoda, Denso Corporation

Three Thermal Simulation & Test Innovations for Electronics Equipment Design

Series Car Brake Cooling

Liquid Cooling Turned on its Side

Thermal Analysis of an ADAS Camera

Thermal Design Leading the Charge

Understanding Die Attach Thermal Performance

Rapid Beverage Cooling Analysis

Bitcoin Mining: A Thermal Perspective

Designing High Efficiency, Low-Cost Synchronous Reluctance Motors

From Measurements to Standardized Multi-Domain Compact Models of LEDs

A Cool Emulator

Achieving Precision in 1D Dynamic Models of Hydraulic Servo Valves

Using FloEFD as an Engineering Tool

Comparison between Experimental & Computational Results

Design of a High Speed Decoy UAV

Thermal Interface for Pluggable Optics Modules

Geek Hub: What do Engineers see in Coffee Grounds?

兆水科技應用案例